METEOROLOGICAL APPLICATIONS
Meteorol. Appl. **18**: 296–306 (2011)
Published online in Wiley Online Library
(wileyonlinelibrary.com) DOI: 10.1002/met.287

RMetS
Royal Meteorological Society

Review

Remote sensing land surface temperature for meteorology and climatology: a review

Charlie J. Tomlinson,[a]* Lee Chapman,[b] John E. Thornes[b] and Christopher Baker[a]
[a] *Department of Civil Engineering, University of Birmingham, Birmingham B15 2TT, UK*
[b] *Department of Geography, Earth and Environmental Sciences, University of Birmingham, Birmingham B15 2TT, UK*

ABSTRACT: The last decade has seen a considerable increase in the amount and availability of remotely sensed data. This paper reviews the satellites, sensors and studies relevant to land surface temperature measurements in the context of meteorology and climatology. The focus is on using the thermal infrared part of the electromagnetic spectrum for useful measurements of land surface temperature, which can be beneficial for a number of uses, for example urban heat island measurements. Copyright © 2011 Royal Meteorological Society

KEY WORDS LST; remote sensing; UHI; satellite; MODIS; Landsat

Received 30 June 2011; Revised 15 July 2011; Accepted 20 July 2011

1. Introduction

Remote sensing is defined as 'the science and art of obtaining information about an object, area, or phenomenon through the analysis of data acquired by a device that is not in contact with the object, area or phenomenon under investigation' (Lillesand *et al*., 2004). The general term originated in the 1960s at a similar time to the launch of the first meteorological satellite, the Television InfraRed Observation Satellite (TIROS-1). Usage is growing within the fields of meteorology and climatology, and works in unison with the use of Geographical Information Systems (GIS) (Chapman and Thornes, 2003; Dyras *et al*., 2005) for spatial analysis. Techniques can provide increased spatial coverage when compared to weather station data (Mendelsohn *et al*., 2007) and the instantaneous observations, global coverage and improving quality of remotely sensed information is proving increasingly useful (Jin and Shepherd, 2005). Remote sensing offers the ability to work at a number of scales, from local/citywide (Tomlinson *et al*., in press), national (Imhoff *et al*., 2010) and worldwide (Jin, 2004). Regardless of the scale of the study, remote sensing offers an opportunity to provide a consistent and repeatable methodology, suited equally to both quick pilot studies as well as long term monitoring campaigns. Although the initial cost of remote sensing platforms is high, the ease of data availability to end researchers, combined with the often extensive temporal and spatial coverage available, offers a marked improvement to traditional fieldwork campaign studies.

This review looks at remote sensing as a tool for meteorology and climatology, with a particular focus on using remotely sensed data to calculate land surface temperature (LST). In this field, the urban heat island (UHI) is a well-documented phenomenon (see reviews by Arnfield (2003), Rizwan *et al*. (2008) and Stewart (2010)) whereby the climate is unintentionally modified, causing urban areas to be warmer than surrounding rural areas. The UHI was first investigated through satellite techniques in the 1970s (Matson *et al*., 1978; Price, 1979), but the field is constantly advancing as new developments in technology (increases in sensor resolution, satellite availability, global coverage, verification methods) and increased understanding of scientific processes come together. Exploration of the UHI effect *via* satellite techniques is the primary focus of this review and specific studies will be discussed under relevant sensor headings. Other uses, such as calculating cooling degree-days (Stathopoulou *et al*., 2006) or monitoring heatwaves (Dousset *et al*., 2010), the impact of urban development on runoff (Herb *et al*., 2008) and soil surface moisture (Petropoulos *et al*., 2009) have also been successfully demonstrated. Remotely sensed data can be a useful resource for the modelling community; helping to define input data such as short wave net radiation for land surface models (Kim and Liang, 2010), or increasing the utility of surface energy balance (Senay *et al*., 2007) and other climate models (Jin *et al*., 2007). A number of reviews exist in this general area. For example, see Kidd *et al*. (2009) for an excellent general overview of

* Correspondence to: C. J. Tomlinson, Department of Civil Engineering, University of Birmingham, Birmingham B15 2TT, UK.
E-mail: cjt512@bham.ac.uk

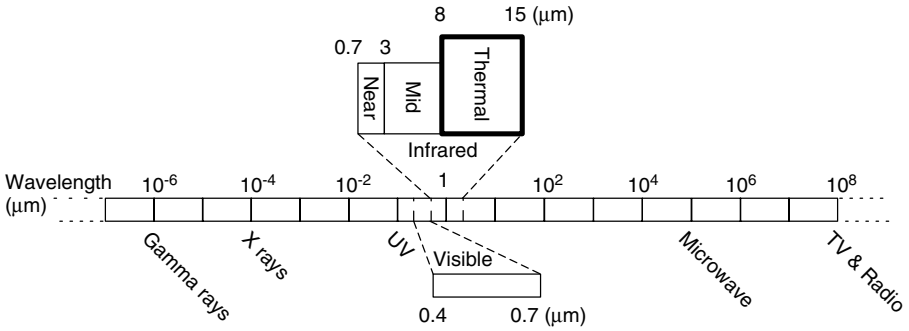

Figure 1. The electromagnetic spectrum arranged by wavelength. Thermal infrared highlighted in bold. Adapted from Lillesand *et al.* (2004).

satellite meteorology and climatology at the start of the twenty-first century. With respect to LST, other reviews have covered satellite remote sensing of the UHI (Gallo *et al.*, 1995), the physics, methods and theoretical limitations of LST retrieval (Dash *et al.*, 2001) and Thermal InfraRed (TIR) remote sensing (Prata, 1994; Voogt and Oke, 2003; Weng, 2009). This review differs from other articles as it details multiple sources of data (including timing and availability). It is written with a meteorologist in mind rather than a remote sensing expert so as such it purposefully does not detail software (either commercial or open source) or in-depth techniques required to use the datasets described.

2. Derivation of land surface temperature

This section outlines the theory behind deriving LST from remote sensing techniques, and covers some fundamental details that need to be understood if data are to be used accurately and usefully for sensing the weather. If more detailed information is required, the physics behind deriving LST is explained in more detail in Dash *et al.* (2002). Several textbooks are also available (e.g. Lillesand *et al.*, 2004). Alternatively, the specification documents of individual sensors or platforms can be inspected (see links in Table II).

A fundamental requirement for remote sensing is the detection of electromagnetic radiation (EMR) by sensors on a remote sensing platform. This is useful as different objects emit EMR in different ways, so the spectral response can be analysed. Within the EMR spectrum (Figure 1), the wavelength of most use for LST measurements is the thermal infrared (TIR), between 8 and 15 μm. However, one exception to this is passive microwave which has been used for LST measurement in China (Chen *et al.*, 2010), USA (McFarland *et al.*, 1990), Canadian sub-arctic (Fily, 2003) and indeed globally (Peterson *et al.*, 2000; Williams *et al.*, 2000). Passive microwave measurements tend to be limited in the sense that they typically offer a very coarse resolution (in the tens of kilometres). For this reason, this review will focus on TIR sensors, which are more commonly used and offer higher resolution data.

Satellite TIR sensors receive EMR which can be quantified in the form of measurements of Top Of Atmosphere (TOA) radiances. This includes upwelling radiance emitted from the ground, upwelling radiance from the atmosphere, and the downwelling radiance emitted by the atmosphere and reflected from the ground. During the day there is both emission and reflection of EMR, but during the night sensed EMR is restricted to only emission. The inverse of Planck's law (the energy emitted by a surface is directly related to its temperature) is used to derive blackbody/brightness temperatures from TOA radiances. TOA radiances are then converted to LST by correcting for three main effects; atmospheric attenuation, angular effects and spectral emissivity values at the surface. Atmospheric attenuation (absorption, reflection or refraction and scattering) will alter the EMR as it passes through the atmosphere, resulting in differences between TOA radiances and LST. Within TIR wavelengths, most attenuation is due to water vapour and aerosols. Angular effects are a product of the variety in viewing angles resulting in wavelength shifting which must be compensated for when estimating radiances (Dash *et al.*, 2002). Spectral emissivity refers to the relative ability of a surface to emit radiation and can be highly variable due to the heterogeneity of land, and is influenced by surface cover, vegetation cover and soil moisture. Quantification of emissivity is achieved by considering the ratio of energy emitted by a surface with respect to the energy emitted by a black body at the same temperature. However, calculations are complicated because natural surfaces do not behave like a black body and thus need correction using typical emissivity values (Table I). These corrections are done through complex algorithms, alongside extensive validation and verification, resulting in a final product that can be used by a meteorologist.

Orbital satellite remote sensing methods are limited by image acquisition time which is set by the orbital characteristics of the relevant satellite and means that readings at specific times cannot be obtained or requested unless they match the orbit. Geostationary satellites, which stay in the same position relative to the Earth, offer a greatly increased temporal resolution at the expense of reducing spatial resolution and coverage area. Examples of sensors on geostationary platforms covered in this review include GOES and SEVERI sensors. However, not all images may be accurate, as high zenith angles result in a lengthened atmospheric path that can result

Table I. Typical emissivity values of common materials (Lillesand *et al.*, 2004).

Material	Typical average emissivity (over 8–14 μm)
Wet snow	0.98–0.99
Healthy green vegetation	0.96–0.99
Wet soil	0.95–0.98
Brick	0.93–0.94
Wood	0.93–0.94
Dry vegetation	0.88–0.94
Dry snow	0.85–0.90
Glass	0.77–0.81
Aluminium foil	0.03–0.07

in less accurate images (Streutker, 2003). Many images come with additional metadata (such as quality control scientific data sets) that can help recognize this problem. It is also worth noting that not all images are readily available, despite orbital paths. Archives may be corrupt, or the satellite may have been offline or manoeuvering in such a way that meant observations were not collected. Hence, if a study has a specific temporal requirement it can therefore be useful to check multiple potential sources. Choice of image timing is also important. For example, Rigo *et al*. (2006) found that MODIS LST was more accurate at night compared to the daytime, and the AATSR target accuracy is 2.5 K for daytime, increasing to 1 K at night time (Noyes *et al*., 2007). Similarly, Hartz *et al*. (2006) found night time ASTER images could better observe neighbourhood climatic conditions. Limitations of resolution are being investigated, and algorithms have been developed to sharpen thermal images to increase the resolution (Dominguez *et al*., 2011). A serious limitation of TIR satellite remote sensing techniques is the requirement for clear skies in order to derive accurate readings. Hence, cloud cover can be a serious problem. Dependent on the research requirements, composite images from multiple passes can often be created in order to construct an image without cloud cover limitations (Neteler, 2010), or algorithms can be used to estimate pixels (Jin and Dickinson, 2000). Alternatively, modelling or passive microwave remote sensing could be used (Wan, 2008) if increased coverage is required. An effect of this is that seasonal differences can influence image availability (increased cloud cover) and accuracy (increased rainfall causing wet surfaces leading to unreliable LST measurements), for example winter study periods can be more difficult (Rajasekar and Weng, 2008).

Two main algorithmic approaches are used for conversions, the radiative transfer equation (RTE) and the generalized split window technique (GSW). These techniques are explained in detail elsewhere (Dash *et al*., 2001; Weng, 2009) and as such are not covered in detail here. The GSW technique in the 11 and 12 μm channels is used by AATSR, AVHRR, MODIS and SEVIRI products, and in simple terms uses adjacent channels with different properties to calculate atmospheric attenuation. Nine different split window algorithms have been evaluated (Yu *et al*., 2008), concluding that accuracies are dependent on having reliable *a priori* emissivity data. This is one difficulty with remotely sensed imagery covering large areas: assumptions of average emissivity across a heterogeneous area. It is important to note that single channel products such as Landsat TM/ETM+ cannot use a GSW technique, and are therefore generally considered less accurate as they will not be correcting for atmospheric attenuation at the time of overpass, although under certain conditions single window methods can provide a reasonable estimate of LST (Platt and Prata, 1993).

The differences between satellite derived LST and ground measured air temperature is one area that is still not fully understood, and is the subject of ongoing work. Reviews (Arnfield, 2003; Weng, 2009) cite research that details both similarities between air and LST (Nichol, 1994) and differences (Weller and Thornes, 2001). Related work includes comparing LST and air temperatures over large areas and multiple ecosystems in Africa (Vancutsem *et al*., 2010) and using MODIS LST data to estimate air temperature in China (Yan *et al*., 2009).

3. Satellites and LST sensors

There is a number of different satellite remote sensing platforms with multiple sensors in the TIR spectrum, giving the modern meteorologist a number of potentially useful datasets to measure LST. Datasets are available for different time periods, at different resolutions, with varying accuracy, therefore this section outlines the various datasets available, ordered by launch date (Figure 2). Currently operating satellites are also summarized in Table II. Some comparisons between datasets exist, for example between MODIS and ASTER (Pu *et al*., 2006) and these are discussed as appropriate. This review will focus on satellite based sensors, as they offer global coverage and good availability. Airborne sensors (e.g. ATLAS (Gluch *et al*., 2006) or AHS (Sobrino *et al*., 2006)) can offer greater spatial and thermal resolution, but generally airborne data are only available for small areas and at significant cost to the end user. Similarly this paper does not detail private or commercial satellites, as these are generally not as accessible for researchers.

3.1. AVHRR

The Advanced Very High Resolution Radiometer (AVHRR) sensor has been on a number of National Oceanic and Atmospheric Administration (NOAA) satellites and is currently operational on NOAA-15,-16,-17,-18 and 19, offering at least daily coverage, but restricted to daytime images. The spatial resolution is ∼1.1 km and LST is derived from TIR channels 4 (10.3–11.3 μm) and 5 (11.5–12.5 μm), with a global dataset provided

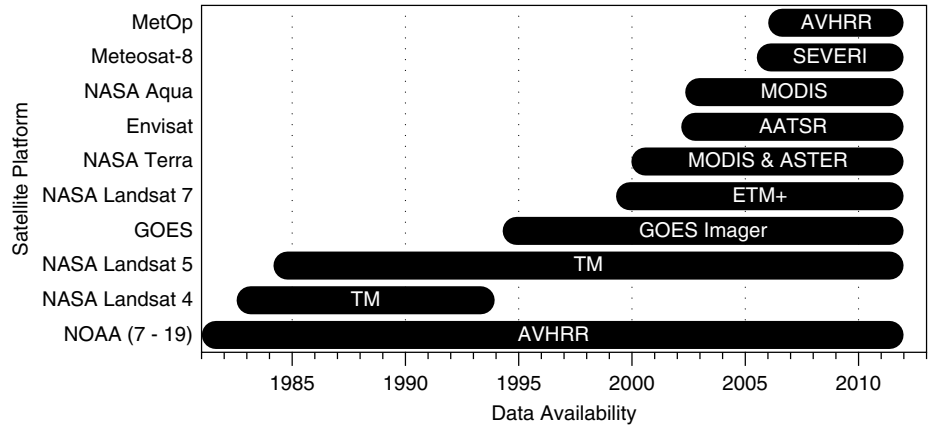

Figure 2. Timeline of satellite launches and associated sensor data availability. Data availability to 2012 indicates ongoing availability.

through the sun-synchronous orbit. Data are available from the NOAA Comprehensive Large Array Stewardship System (http://www.nsof.class.noaa.gov/saa/) and the High Resolution Picture Transmission software (http://www.satsignal.eu/software/hrpt.htm) can be useful for analysis. MetOP, the EUMETSAT satellite platform, also has an AVHRR sensor with an orbital repeat time of 29 days. Comparative studies of AVHRR algorithms exist which offer more details (Ottle and Vidal-Madjar, 1992; Vázquez *et al*., 1997).

A strength of the AVHRR sensor is that there is a relatively long historical record of data, and correspondingly a significant body of research that has used the sensor for many different uses. A notable use of AVHRR data has been in the creation of an 18 year (1981–1998) diurnal LST dataset (Jin, 2004) at 8 km resolution globally for snow free land surfaces. It gives monthly diurnally-averaged, minimum and maximum skin temperatures. This long term record is not possible with most other sensors as the historical data are not available, as the satellites and sensors were not developed or in space. Matson *et al*. (1978) used VHRR (the forerunner to AVHRR) data for UHI analysis of the US, detecting over 50, and LST investigations in Northern Italy used AVHRR (Ulivieri and Cannizzaro, 1985). Other studies using AVHRR include Gallo *et al*. (1993) who investigated the surface temperature and vegetation index for 37 cities in the United States, particularly noting the consistent nature of the data when studying UHI. Lee (1993) used AVHRR to study the UHI in South Korea and more recently AVHRR data have been used to study the growth of the UHI in Houston, Texas, USA between 1985–1987 and 1999–2001, with the results showing a growth in magnitude of 35%, and a growth in area between 38 and 88% depending on method (Streutker, 2003). Stathopoulou and Cartalis (2009) used AVHRR data from Greece and applied downscaling techniques to increase the output resolution (1 km >120 m), helping to address the inevitable balancing between spatial and temporal resolution. A significant weakness of AVHRR includes the lack of availability of night time images.

3.2. Landsat

The Landsat series of satellites are probably the most well known, with the longest record of Earth observations from space. The Thematic Mapper (TM) on Landsat 4 and 5 had a visible resolution of 30 m and a TIR resolution of 120 m (band 6, 10.4–12.5 μm). Landsat 4 and 5 are no longer continually collecting data, but Landsat 7's Enhanced Thematic Mapper (ETM+) collects thermal data at a 60 m resolution (also band 6, 10.4–12.5 μm). Landsat 7 has a near polar Sun-synchronous orbit with a revisit time of 16 days, meaning that a given point on Earth should be imaged at approximately the same local time (∼1000 h) every 16 days. The ETM+ offers some of the highest resolution thermal resolution measurements from space, and data are available freely from the U.S. Geological Survey (USGS) (http://earthexplorer.usgs.gov/or http://glovis.usgs.gov), however data from 2003 onwards are impaired due to failure of the scan line corrector. This results in only ∼80% of each scene being captured. The Landsat data archive has only been freely available since 2008, therefore the number of studies has increased in recent years. A disadvantage of data from Landsat is that they are not collected at night, and the thermal calibration is limited. More details on the Landsat project is available (http://pubs.usgs.gov/fs/2010/3026) and the Landsat Data Continuity Mission (LCDM) aims to continue the long term Landsat record.

In the USA, Aniello *et al*. (1995) used Landsat TM data to help map micro UHIs (hot spots within a city) in Dallas, Texas, USA by combining both the thermal band (6) and extracted tree cover data from an unsupervised classification. One satellite image was used and the results showed that micro UHIs were highest in the centre and were generally resulting from a lack of tree cover. Weng *et al*. (2004) use Landsat ETM+ to link LST to Normalized Difference Vegetation Index (NDVI) in Indianapolis, USA which resulted in results linking LST to different land cover types and Xian and Crane (2006) use both Landsat TM and ETM+ to explore the thermal characteristics of urban areas in Tampa Bay and Florida, USA finding that land use and land cover fundamentally

Table II. Current LST capable sensors and satellite information.

Sensor	Satellite	Spatial resolution	Orbital frequency	TIR spectral bands (μm)	Image acquisition (local time)	Data available since	Website
Landsat ETM+	Landsat 7	60 m[a]	16 days	(6) 10.4–12.5	~1000	1999[b]	http://pubs.usgs.gov/fs/2010/3026/ http://landsat.gsfc.nasa.gov/
MODIS	Aqua	~1 km	Twice daily	(31) 10.78–11.28 (32) 11.77–12.27	~1330 ~0130	2002	http://modis.gsfc.nasa.gov/ https://lpdaac.usgs.gov/lpdaac/products/modis_overview
MODIS	Terra	~1 km	Twice daily	(31) 10.78–11.28 (32) 11.77–12.27	~1030 ~2230	2000 2000	http://modis.gsfc.nasa.gov/ https://lpdaac.usgs.gov/lpdaac/products/modis_overview
ASTER	Terra	90 m	Twice daily	(10) 8.125–8.475 (11) 8.475–8.825 (12) 8.925–9.275 (13) 10.25–10.95 (14) 10.95–11.65	Request only	1999	http://asterweb.jpl.nasa.gov/index.asp
AVHRR	Multiple NOAA	~1.1 km	Twice daily	(4) 10.3–11.3 (5) 11.5–12.5[c]	[d]	1979	http://noaasis.noaa.gov/NOAASIS/ml/avhrr.html http://eros.usgs.gov/#/Find_Data/Products_and_Data_Available/AVHRR
AVHRR	MetOP	~1.1 km	29 days	(4) 10.3–11.3 (5) 11.5–12.5	~0930	2006	http://www.esa.int/esaLP/ESA7USVTYWC_LPmetop_0.html
AATSR	Envisat	~1 km	35 days	11 12	~1000	2004[e]	http://envisat.esa.int/instruments/aatsr/
SEVIRI	Meteosat-8	~3 km	Geostationary	10.8 12	Every 15 min	2005	http://landsaf.meteo.pt/
GOES Imager	GOES network[f]	~4 km	Geostationary	(4) 10.2–11.2 (5) 11.5–12.5	Every 3 h (full disc)	1974	http://goespoes.gsfc.nasa.gov/goes/index.html

[a] Collected at 60 m but resampled to 30 m.
[b] Landsat 7 ETM+ data from 1999, TM data from Landsat 4 and 5 available since 1982 at 120 m spatial resolution.
[c] AVHRR/3 characteristics.
[d] AVHRR is carried on >10 NOAA satellites; see http://ivm.cr.usgs.gov/tables.php for full orbital details of each.
[e] LST product currently available since 2004. Planned application to historical data will result in data from 1991 onwards.
[f] Status of network available: http://www.oso.noaa.gov/goesstatus/.

affect the thermal results. Weng (2003) used three Landsat TM images (from 1989, 1996 and 1997) to study the UHI in Guangzhou, China alongside fractal analysis with the result that showed two significant heat islands existed in the city. Further work has been done in China (Chen *et al*., 2006; Li *et al*., 2009), including combining Landsat ETM+ with computational fluid dynamic (CFD) modelling in Wuhan, China (Li and Yu, 2008). The combination of remote sensing and modelling was found to be mutually complementary. In Europe, Stathopoulou and Cartalis (2007) used Landsat ETM+ data to explore the daytime UHI across the major cities in Greece using a method that incorporates the CORINE land cover classification to superimpose land cover based emissivity values to create a mean surface temperature by land cover.

Resampling (generally using the nearest neighbour algorithm) the thermal band to lower resolutions (e.g. 30 m to match the visible spectrum) is a common technique (Weng, 2003; Weng *et al*., 2004; Xian and Crane, 2006; Cao *et al*., 2010) in order to simplify analysis. Landsat has a great strength in terms of spatial resolution, however its 16 day revisit time and lack of night time image acquisition is limiting at the temporal scale. Stathopoulou and Cartalis (2007) discusses how future studies may focus on a time series of images as the UHI strongly depends on synoptic weather conditions. The spatial resolution of 60 m on Landsat ETM+ does allow individual hotspots to be picked out (Aniello *et al*., 1995; Stathopoulou and Cartalis, 2007) and work is still using the ETM+ sensor (Boudhar *et al*., 2011).

3.3. GOES

The Geostationary Operational Environmental Satellite (GOES) system is a network of geostationary satellites (status available: http://www.oso.noaa.gov/goesstatus/) carrying the GOES Imager, a multispectral instrument offering two channels in the TIR (10.2–11.2 and 11.5–12.5 μm) with an at nadir resolution of ~4 km. GOES related studies discuss algorithm development for

dual thermal channel sensors (e.g. on GOES-8 and -10) (Sun, 2003) and single thermal channel sensors (e.g. GOES M-Q) (Sun *et al*., 2004). An evaluation of GOES LST retrievals over the USA is given by Pinker *et al.* (2009). An illustration of an advantage of geostationary satellites is shown by Sun *et al*. (2006), which measures the diurnal temperature range across the USA, possible due to the high temporal availability of data. An interesting study links MODIS data as a calibration source for GOES data, resulting in a 1 km LST dataset at half-hourly temporal resolution and a measured accuracy better than 2 °C (Inamdar *et al*., 2008).

3.4. MODIS

The MODerate resolution Imaging Spectroradiometer (MODIS) sensor is carried on both NASA's Aqua and Terra satellites that have near polar orbits resulting in two images *per* satellite *per* day. Image acquisition on Aqua is ∼1330 and 0130 h and Terra is ∼1030 and 2230 h, all local time. This is a high temporal resolution, and the spatial resolution is ∼1 km. Data are available from the USGS Land Processes Distributed Active Archive Center (https://lpdaac.usgs.gov/) and useful LST products include MYD11A1 (Aqua) and MOD11A1 (Terra) which are the daily LST and emissivity at 1 km. Other products include 8 day 1 km data (M*D11A2) and others. These LST products primarily use TIR bands 31 (10.78–11.28 μm) and 32 (11.77–12.27 μm) combined with split window algorithms (Wan and Dozier, 1996) which multiple studies have tested (Wan, 2002, 2008; Wan *et al*., 2004; Coll *et al*., 2005) with results suggesting accuracies greater than 1 K over homogeneous surfaces. A useful tool for processing data in ESRI ArcMap is the Marine Geospace Ecology Tools (MGET) plugin (Roberts *et al*., 2010), or the standalone MODIS Reprojection Tool (https://lpdaac.usgs.gov/lpdaac/tools/modis_reprojection_tool).

There is a number of studies that use MODIS LST data within the urban climatology fields. Within Europe, Pongrácz *et al*. (2010) explored the UHI of nine central European cities and find that the most intense UHI occurs during daytime in the summer. The summer UHI of Birmingham has been analysed (Tomlinson *et al*., in press) and work has looked at the 10 most populated cities of Hungary (Pongrácz *et al*., 2006). Studies in Bucharest used MODIS to calculate the UHI in summer months (Cheval and Dumitrescu, 2009) and under heatwave conditions (Cheval *et al*., 2009). Globally, Hung *et al.* (2006) quantified the UHI in eight Asian mega-cities using MODIS data, Jin *et al.* (2005) analysed various cities including Beijing and New York, and Imhoff *et al.* (2010) used MODIS data averaged over 3 years to calculate UHIs across the United States.

MODIS data have been used extensively outside the UHI field. Other surface measurements include observing the impacts of agriculture on rural surface temperatures in North America (Ge, 2010) and measuring water temperature and heat flux over a hydroelectric reservoir in Brazil (Alcântara *et al*., 2010). Atmospheric studies estimate aerosol optical depth (an important influence on the radiation budget) in America, Canada, China and Africa (Liang *et al*., 2006), and help detect clear sky, low level temperature inversions in the polar regions (Liu and Key, 2003). In cooler areas, MODIS has been used for frost risk assessment in Bolivia (Pouteau *et al*., 2010) and permafrost monitoring in Siberia (Langer *et al*., 2010). Outside of the meteorology domain, MODIS data have been used to help epidemiological studies of tick-borne diseases (Neteler, 2005) and more. A strength of the MODIS sensor is the compromise between regular image acquisition and reasonable spatial resolution, in comparison to other sensors that offer higher spatial resolution but lower temporal resolution (e.g. Landsat), or higher temporal resolution but lower spatial resolution (e.g. SEVIRI).

3.5. ASTER

The Advanced Spaceborne Thermal Emission and Reflection Radiometer (ASTER) operates at a very high resolution (90 m), and calculates surface temperature (AST08 product – http://asterweb.jpl.nasa.gov/content/03_data/01_Data_Products/SurfaceTemperature.pdf) using the Temperature Emissivity Separation (TES) algorithm (Gillespie and Rokugawa, 1998). ASTER has five TIR bands, and full technical details are available in Yamaguchi *et al.* (1998). ASTER is based on the NASA Terra satellite platform, but is fundamentally different from other sensors discussed in this review in that it is request only, with fees payable for data. Hence, data are only acquired if a specific request has been detailed and paid for, and therefore the historical data are limited and costly. This is a significant restriction, given the difficulties of ensuring suitable atmospheric and weather conditions for a specific future request, and obviously limits historical studies. However, the 90 m resolution is high, only comparable with Landsat when considering the spatial scale, and ASTER has the potential for better temporal coverage, given the Terra satellite has a twice daily pass.

ASTER images have been used for a number of studies. They were used to compare LST to urban biophysical descriptors (such as impervious surface, green vegetation and soil) in Indianapolis, USA through linear spectral mixture analysis and multiple regression models, with the results that impervious surfaces and hot objects were positively correlated with LST, whereas vegetation and cold objects were negatively correlated (Lu and Weng, 2006). An ASTER image was used alongside a 148 km vehicle traverse of Hong Kong in order to compare air and remotely sensed temperatures (Nichol *et al*., 2009) and ASTER (for thermal use) and IKONOS data (for high resolution (4 m) visible and near infrared use) were combined to explore the cooling effect of urban parks in Nagoya, Japan (Cao *et al*., 2010).

There are frequent comparisons between ASTER and MODIS data, for example in verification. This is because

ASTER and MODIS are complementary in scale (∼1 km and 90 m) and are based on the same satellite platform, so image acquisition occurs at the same time, height and location which aids comparison. Land surface emissivity and radiometric temperatures have been compared with good agreement over desert in the USA and savannah in Africa (Jacob *et al*., 2004). Direct comparisons between three correction approaches over the Loess Plateau in China have reduced the discrepancies between ASTER and MODIS data (Liu *et al*., 2007). Long term ground based long wave radiation between 2000 and 2007 have been compared to ASTER and MODIS images for both LST and emissivity (Wang and Liang, 2009).

3.6. AATSR

The Advanced Along Track Scanning Radiometer (AATSR) is carried onboard the European Space Agency (ESA) ENVironment SATellite (ENVISAT) which was launched in 2002. This was the third instrument in a series (ATSR-1 and ATSR-2) which started with the Along Track Scanning Radiometer (ATSR-1) in 1991. The primary objective of all missions to date has been for sea surface temperature (SST) collection. ENVISAT is in a Sun-synchronous polar orbit with a 35 day repeat cycle, which means data availability is lower than others. The LST product is relatively new, being operational from March 2004 for data from the AATSR, and the TIR bands 11 and 12 μm are used to provide LST at ∼1 km resolution. However the algorithms developed will be applied to historical data from the previous sensors (ATSR-1 and ATSR-2) resulting in an LST dataset starting in 1991, although the timeline for completion is unknown. The AATSR literature is primarily concerned with the theoretical science for algorithm development (Prata, 2002), evaluation of algorithms (Sòria and Sobrino, 2007) or validation (Coll *et al*., 2005, 2009; Noyes *et al*., 2007). AATSR has been used for monthly LST mapping over Europe (Joan and Cesar, 2009) and more broadly for drought prediction (Djepa, 2011), estimating evapotranspiration (Liu *et al*., 2010) and detection of snow covered areas (Istomina *et al*., 2010). In the future more studies using AATSR can be anticipated, although the long orbital repeat cycle means other sensors may be better suited.

3.7. SEVIRI

The Spinning Enhanced Visible and Infrared Imager (SEVIRI) is an instrument on Meteosat-8 that uses a generalized split window algorithm (detailed in Sobrino, 2004) to calculate LST from two thermal channels (10.8 and 12 μm). The satellite application facility on land surface analysis (http://landsaf.meteo.pt/) is responsible for generation and archiving of the data. Meteosat Second Generation (MSG) is a geostationary satellite so therefore has different characteristics to other orbital satellites this review has examined. It has a very high temporal resolution of 15 min (theoretical maximum of 96 images *per* day) but the area covered is constant and not global. All the land pixels within the Meteosat disc that are below a 60° viewing angle are processed for LST measurements, to avoid excessive atmospheric attenuation and reduced accuracy at higher angles. This results in a spatial pixel resolution of 3 km at nadir (increasing to ∼6 km at >60°). Schmetz *et al*. (2002) offer a useful introduction to the MSG instrument. The high temporal resolution has a number of advantages, namely it has a much greater chance of getting cloud free images of a study area due to the number that are taken and it enables the potential to study the diurnal LST pattern. Meteosat data have been available since July 2005 for the complete Meteosat disc (February 2005 for Europe).

Trigo *et al*. (2008) compare Meteosat LST with MODIS LST over three locations and find that Meteosat temperatures are warmer than MODIS, particularly in the daytime. A comparison between MODIS and Meteosat LST has also been carried out focussing on the heatwave in Athens, Greece during July 2007 (Retalis *et al*., 2010) and the results show significant correlation both between each other and between air temperature measurements, which agrees with other air temperature and Meteosat LST comparisons that also perform well (Nieto *et al*., 2011).

Due to the high temporal resolution, it is theoretically possible to study the diurnal UHI. In practice this is limited by cloud cover, however recent work outlines a methodology for reconstructing cloud contaminated pixels (Lu *et al*., 2011) that allows the diurnal variation to be studied in detail. In other fields this high temporal resolution is useful, for example for hazard modelling such as near real time forest fire monitoring (Umamaheshwaran *et al*., 2007).

4. Future developments

The future for remote sensing LST retrievals is focussed on two main areas, that of improved or replacement physical sensors and platforms, and that of improvements in data manipulation of current, historical and future data. In terms of data manipulation there is potential for improved algorithms, for example improved cloud masking or emissivity calculations. These will rely on ongoing validation and testing across a variety of landscapes and sensors, and could improve existing as well as future data.

Regarding the near future of sensors and satellite platforms, a number of relevant projects are in development. The Landsat Data Continuity Mission (LDCM) (http://ldcm.nasa.gov/or http://pubs.usgs.gov/fs/2007/3093/) intends to continue the long Landsat data series, and is due to be launched in December 2012 with 120 m resolution in two thermal channels. The European Space Agency (ESA) Sentinel-3 satellites are planned for launch from 2013, offering a Sea and Land Surface Temperature Radiometer (SLSTR) with a 1 km resolution in the thermal channels and a daily revisit time. The geostationary GOES-R satellite is due in 2015,

with a 2 km resolution in the thermal channels from a new Advanced Baseline Imager (ABI) (Yunyue *et al*., 2009). The National Polar-orbiting Operational Environmental Satellite System (NPOESS) is due to launch in 2016, designed to replace NASA's Aqua, Terra and Aura satellites and offering the Visible and Infrared Imagery Radiometer Suite (VIIRS) sensor for LST. An interesting sensor in development is the Hyperspectral InfraRed Imager (HyspIRI) from NASA that is hopefully planned for launch in 2015, offering a ∼60 m resolution in the thermal bands and a repeat cycle of 5 or 16 days. This is still in a planning phase and more details are available online (http://hyspiri.jpl.nasa.gov/) but this offers the next generation of space based thermal sensors. Coupled with these large 'traditional' missions, in the future there is likely to be an increase in 'small satellites' (Sandau *et al*., 2010) that enable relatively quick and inexpensive missions, which could for example help to observe dynamic weather systems. Future increases in spatial resolution of sensors combined with the high temporal resolution that geostationary platforms can provide is likely to offer the most useful data, however this offers considerable scientific challenges.

5. Conclusion

This review has given an overview of remote sensing techniques, sensors and research of interest to the meteorological and climatological community for LST detection and monitoring. It is clear that the focus of research has been surrounding the UHI phenomenon, but a significant research gap still exists which is the quantification of the relationship between measured air temperatures and remotely sensed LST data. Indeed, as Nichol *et al*. (2009) state this 'remains the greatest unknown in remotely sensed studies of heat islands', and this statement is still applicable to any study using LST data as a proxy for air temperature. The importance of being able to relate LST to air temperature is especially important when such datasets are being used to inform policy decisions or communicate outside of the scientific community.

A significant advantage of remote sensing data and techniques is their truly global coverage and scope, but despite this there is a low number of studies focussing on many geographical areas, and a limited number that integrate additional ground data. Remote sensing techniques offer access to data that would otherwise be unobtainable, therefore the requirement for defensible verification and accuracy measurements is considerable. Alongside this, the increasing need for data and intensifying analysis will necessitate using remote sensing data alongside other datasets from numerous sources, resulting in an integral role for remote sensing techniques within the meteorological and climatological communities.

Acknowledgements

This research has been funded by a Doctoral Training Award issued by the Engineering and Physical Sciences Research Council and supported by Birmingham City Council.

List of Acronyms

ATLAS Advanced Thermal and Land Applications Sensor
ATSR Along Track Scanning Radiometer
AVHRR Advanced Very High Resolution Radiometer
CFD Computational Fluid Dynamics
EMR Electromagnetic Radiation
ENVISAT ENVIronment SATellite
ESA European Space Agency
ETM+ Enhanced Thematic Mapper+
EUMETSAT European Organisation for the Exploitation of Meteorological Satellites
GIS Geographical Information Systems
GOES Geostationary Operational Environmental Satellite
GSW Generalised Split Window Technique
HyspIRI Hyperspectral InfraRed Imager
LDCM Landsat Data Continuity Mission
LST Land Surface Temperature
MODIS MODerate resolution Imaging Spectroradiometer
MSG Meteosat Second Generation
NASA National Aeronautics and Space Administration
NDVI Normalized Difference Vegetation Index
NOAA National Oceanic and Atmospheric Administration
NPOESS National Polar-orbiting Operational Environmental Satellite System
RTE Radiative Transfer Equation
SEVIRI Spinning Enhanced Visible and Infrared Imager
SLSTR Sea and Land Surface Temperature Radiometer
SST Sea Surface Temperature
TES Temperature Emissivity Separation
TIR Thermal InfraRed
TIROS-1 Television InfraRed Observation Satellite
TM Thematic Mapper
TOA Top of Atmosphere
UHI Urban Heat Island
USGS United States Geological Survey
VHRR Very High Resolution Radiometer
VIIRS Visible and Infrared Imagery Radiometer Suite

References

Alcântara EH, Stech JL, Lorenzzetti JA, Bonnet MP, Casamitjana X, Assireu AT, Novo EMDM. 2010. Remote sensing of water surface temperature and heat flux over a tropical hydroelectric reservoir. *Remote Sensing of Environment* **114**: 2651–2665.

Aniello C, Morgan K, Busbey A, Newland L. 1995. Mapping micro-urban heat islands using Landsat TM and a GIS. *Computers and Geosciences* **21**: 965–967.

Arnfield A. 2003. Two decades of urban climate research: a review of turbulence, exchanges of energy and water, and the urban heat island. *International Journal of Climatology* **23**: 1–26.

Boudhar A, Duchemin B, Hanich L, Boulet G, Chehbouni A. 2011. Spatial distribution of the air temperature in mountainous areas using satellite thermal infra-red data. *Comptes Rendus Geoscience* **343**: 32–42.

Cao X, Onishi A, Chen J, Imura H. 2010. Quantifying the cool island intensity of urban parks using ASTER and IKONOS data. *Landscape and Urban Planning* **96**: 224–231.

Chapman L, Thornes JE. 2003. The use of geographical information systems in climatology and meteorology. *Progress in Physical Geography* **27**: 313–330.

Chen S-S, Chen X-Z, Chen W-Q, Su Y-X, Li D. 2011. A simple retrieval method of land surface temperature from AMSR-E passive microwave data – a case study over Southern China during the strong snow disaster of 2008. *International Journal of Applied Earth Observations and Geoinformation* **13**: 140–151.

Chen X, Zhao H, Li P, Yin Z. 2006. Remote sensing image-based analysis of the relationship between urban heat island and land use/cover changes. *Remote Sensing of Environment* **104**: 133–146.

Cheval S, Dumitrescu A. 2009. The July urban heat island of Bucharest as derived from modis images. *Theoretical and Applied Climatology* **96**: 145–153.

Cheval S, Dumitrescu A, Bell A. 2009. The urban heat island of Bucharest during the extreme high temperatures of July 2007. *Theoretical and Applied Climatology* **97**: 391–401.

Coll C, Caselles V, Galve J, Valor E, Niclos R, Sanchez J, Rivas R. 2005. Ground measurements for the validation of land surface temperatures derived from AATSR and MODIS data. *Remote Sensing of Environment* **97**: 288–300.

Coll C, Hook SJ, Galve JM. 2009. Land surface temperature from the advanced along-track scanning radiometer: validation over inland waters and vegetated surfaces. *IEEE Transactions on Geoscience and Remote Sensing* **47**: 350–360.

Dash P, Göttsche F, Olesen F, Fischer H. 2001. Retrieval of land surface temperature and emissivity from satellite data: physics, theoretical limitations and current methods. *Journal of the Indian Society of Remote Sensing* **29**: 23–30.

Dash P, Gottsche FM, Olesen FS, Fischer H. 2002. Land surface temperature and emissivity estimation from passive sensor data: theory and practice-current trends. *International Journal of Remote Sensing* **23**: 2563–2594.

Djepa V. 2011. Drought prediction using the Along Track Scanning Radiometer (ATSR2) on board ERS2 satellite. *Advances in Space Research* **48**: 56–60.

Dominguez A, Kleissl J, Luvall JC, Rickman DL. 2011. High-resolution urban thermal sharpener (HUTS). *Remote Sensing of Environment* **115**: 1772–1780.

Dousset B, Gourmelon F, Laaidi K, Zeghnoun A, Giraudet E, Bretin P, Mauri E, Vandentorren S. 2010. Satellite monitoring of summer heat waves in the Paris metropolitan area. *International Journal of Climatology* **31**: 313–323.

Dyras I, Dobesch H, Grueter E, Perdigao A, Tveito O, Thornes JE, van der Wel F, Bottai L. 2005. The use of geographic information systems in climatology and meteorology: COST 719. *Meteorological Applications* **12**: 1–5.

Fily M. 2003. A simple retrieval method for land surface temperature and fraction of water surface determination from satellite microwave brightness temperatures in sub-arctic areas. *Remote Sensing of Environment* **85**: 328–338.

Gallo K, McNab A, Karl T, Brown J, Hood J, Tarpley J. 1993. The use of NOAA AVHRR data for assessment of the urban heat-island effect. *Journal of Applied Meteorology* **32**: 899–908.

Gallo K, Tarpley J, McNab A, Karl T. 1995. Assessment of urban heat islands: a satellite perspective. *Atmospheric Research* **37**: 37–43.

Ge J. 2010. MODIS observed impacts of intensive agriculture on surface temperature in the southern Great Plains. *International Journal of Climatology* **30**: 1994–2003.

Gillespie A, Rokugawa S. 1998. A temperature and emissivity separation algorithm for Advanced Spaceborne Thermal Emission and Reflection Radiometer (ASTER) images. *IEEE Transactions on Geoscience and Remote Sensing* **36**: 1113–1126.

Gluch R, Quattrochi D, Luvall J. 2006. A multi-scale approach to urban thermal analysis. *Remote Sensing of Environment* **104**: 123–132.

Hartz D, Prashad L, Hedquist B, Golden J, Brazel A. 2006. Linking satellite images and hand-held infrared thermography to observed neighborhood climate conditions. *Remote Sensing of Environment* **104**: 190–200.

Herb W, Janke B, Mohseni O. 2008. Ground surface temperature simulation for different land covers. *Journal of Hydrology* **356**: 327–343.

Hung T, Uchihama D, Ochi S, Yasuoka Y. 2006. Assessment with satellite data of the urban heat island effects in Asian mega cities. *International Journal of Applied Earth Observation and Geoinformation* **8**: 34–48.

Imhoff M, Zhang P, Wolfe R, Bounoua L. 2010. Remote sensing of the urban heat island effect across biomes in the continental USA. *Remote Sensing of Environment* **114**: 504–513.

Inamdar AK, French A, Hook S, Vaughan G, Luckett W. 2008. Land surface temperature retrieval at high spatial and temporal resolutions over the southwestern United States. *Journal of Geophysical Research* **113**: 1–18.

Istomina LG, von Hoyningen-Huene W, Kokhanovsky AA, Burrows JP. 2010. The detection of cloud-free snow-covered areas using AATSR measurements. *Atmospheric Measurement Techniques* **3**: 1005–1017.

Jacob F, Petitcolin F, Schmugge T, Vermote É, French A, Ogawa K. 2004. Comparison of land surface emissivity and radiometric temperature derived from MODIS and ASTER sensors. *Remote Sensing of Environment* **90**: 137–152.

Jin M. 2004. Analysis of land skin temperature using AVHRR observations. *Bulletin of the American Meteorological Society* **85**: 587–600.

Jin M, Dickinson R. 2000. A generalized algorithm for retrieving cloudy sky skin temperature from satellite thermal infrared radiances. *Journal of Geophysical Research* **105**(27): 27037–27047.

Jin M, Dickinson R, Zhang D. 2005. The footprint of urban areas on global climate as characterized by MODIS. *Journal of Climate* **18**: 1551–1565.

Jin M, Shepherd JM. 2005. Inclusion of urban landscape in a climate model: how can satellite data help? *Bulletin of the American Meteorological Society* **86**: 681–689.

Jin M, Shepherd JM, Peters-Lidard C. 2007. Development of a parameterization for simulating the urban temperature hazard using satellite observations in climate model. *Natural Hazards* **43**: 257–271.

Joan M, Cesar C. 2009. Monthly land surface temperature maps over European zone using advanced along track scanning radiometer data for 2007. *Geoscience and Remote Sensing Symposium, 2009 IEEE International, IGARSS 2009*, **4:** 292–295.

Kidd C, Levizzani V, Bauer P. 2009. A review of satellite meteorology and climatology at the start of the twenty-first century. *Progress in Physical Geography* **33**: 474–489.

Kim H-Y, Liang S. 2010. Development of a hybrid method for estimating land surface short wave net radiation from MODIS data. *Remote Sensing of Environment* **114**: 2393–2402.

Langer M, Westermann S, Boike J. 2010. Spatial and temporal variations of summer surface temperatures of wet polygonal tundra in Siberia – implications for MODIS LST based permafrost monitoring. *Remote Sensing of Environment* **114**: 2059–2069.

Lee H. 1993. An application of NOAA AVHRR thermal data to the study of urban heat islands. *Atmospheric Environment. Part B: Urban Atmosphere* **27**: 1–13.

Li J-J, Wang X-R, Wang X-J, Ma W-C, Zhang H. 2009. Remote sensing evaluation of urban heat island and its spatial pattern of the Shanghai metropolitan area, China. *Ecological Complexity* **6**: 413–420.

Li K, Yu Z. 2008. Comparative and combinative study of urban heat island in Wuhan City with remote sensing and CFD simulation. *Sensors* **8**: 6692–6703.

Liang S, Zhong B, Fang H. 2006. Improved estimation of aerosol optical depth from MODIS imagery over land surfaces. *Remote Sensing of Environment* **104**: 416–425.

Lillesand T, Kiefer R, Chipman J. 2004. *Remote Sensing and Image Interpretation*. John Wiley: Chichester.

Liu Y, Key J. 2003. Detection and analysis of clear-sky, low-level atmospheric temperature inversions with MODIS. *Journal of Atmospheric and Oceanic Technology* **20**: 1727–1737.

Liu R, Wen J, Wang X, Wang L, Tian H, Zhang T, Shi X, Zhang J, LV S. 2010. Actual daily evapotranspiration estimated from MERIS and AATSR data over the Chinese Loess Plateau. *Hydrology and Earth System Sciences* **14**: 47–58.

Liu Y, Yamaguchi Y, Ke C. 2007. Reducing the discrepancy between ASTER and MODIS land surface temperature products. *Sensors* **7**: 3043–3057.

Lu L, Venus V, Skidmore A, Wang T, Luo G. 2011. Estimating land-surface temperature under clouds using MSG/SEVIRI observations. *International Journal of Applied Earth Observations and Geoinformation* **13**: 265–276.

Lu D, Weng Q. 2006. Spectral mixture analysis of ASTER images for examining the relationship between urban thermal features

and biophysical descriptors in Indianapolis, Indiana, USA. *Remote Sensing of Environment* **104**: 157–167.
McFarland MJ, Miller RL, Neale CMU. 1990. Land surface temperature derived from the SSM/I passive microwave brightness temperatures. *IEEE Transactions on Geoscience and Remote Sensing* **28**: 839–845.
Matson M, Mcclain E, McGinnis D Jr, Pritchard J. 1978. Satellite detection of urban heat islands. *Monthly Weather Review* **106**: 1725–1734.
Mendelsohn R, Kurukulasuriya P, Basist A, Kogan F, Williams C. 2007. Climate analysis with satellite versus weather station data. *Climatic Change* **81**: 71–83.
Neteler M. 2005. Time series processing of MODIS satellite data for landscape epidemiological applications. *International Journal of Geoinformatics* **1**: 133–138.
Neteler M. 2010. Estimating daily land surface temperatures in mountainous environments by reconstructed MODIS LST data. *Remote Sensing* **2**: 333–351.
Nichol JE. 1994. A GIS-based approach to microclimate monitoring in Singapore's high-rise housing estates. *Photogrammetric Engineering and Remote Sensing* **60**: 1225–1232.
Nichol JE, Fung WY, Lam K-S, Wong MS. 2009. Urban heat island diagnosis using ASTER satellite images and 'in situ' air temperature. *Atmospheric Research* **94**: 276–284.
Nieto H, Sandholt I, Aguado I, Chuvieco E, Stisen S. 2011. Air temperature estimation with MSG-SEVIRI data: calibration and validation of the TVX algorithm for the Iberian Peninsula. *Remote Sensing of Environment* **115**: 107–116.
Noyes E, Sòria G, Sobrino J, Remedios J. 2007. AATSR land surface temperature product algorithm verification over a WATERMED site. *Advances in Space Research* **39**: 171–178.
Ottle C, Vidal-Madjar D. 1992. Estimation of land surface temperature with NOAA9 data. *Remote Sensing of Environment* **40**: 27–41.
Peterson T, Basist A, Williams C. 2000. A blended satellite–in situ near–global surface temperature dataset. *Bulletin of the American Meteorological Society* **81**: 2157–2164.
Petropoulos G, Carlson T, Wooster M, Islam S. 2009. A review of Ts/VI remote sensing based methods for the retrieval of land surface energy fluxes and soil surface moisture. *Progress in Physical Geography* **33**: 224–250.
Pinker RT, Sun D, Hung M-P, Li C, Basara JB. 2009. Evaluation of satellite estimates of land surface temperature from GOES over the United States. *Journal of Applied Meteorology and Climatology* **48**: 167–180.
Platt CMR, Prata AJ. 1993. Nocturnal effects in the retrieval of land surface temperatures from satellite measurements. *Remote Sensing of Environment* **45**: 127–136.
Pongrácz R, Bartholy J, Dezso Z. 2006. Remotely sensed thermal information applied to urban climate analysis. *Advances in Space Research* **37**: 2191–2196.
Pongrácz R, Bartholy J, Dezsö Z. 2010. Application of remotely sensed thermal information to urban climatology of Central European cities. *Physics and Chemistry of the Earth* **35**: 95–99.
Pouteau R, Rambal S, Ratte J, Gogé F, Joffre R, Winkel T. 2010. Downscaling MODIS-derived maps using GIS and boosted regression trees: the case of frost occurrence over the arid Andean highlands of Bolivia. *Remote Sensing of Environment* **115**: 117–129.
Prata A. 1994. Land surface temperature determination from satellites. *Advances in Space Research* **14**: 15–26.
Prata A. 2002. *Land Surface Temperature Measurement from Space: AATSR Algorithm Theoretical Basis Document*. Contract Report to ESA. CSIRO Atmospheric Research: Aspendale; 1–34.
Price J. 1979. Assessment of the urban heat island effect through the use of satellite data. *Monthly Weather Review* **107**: 1554–1557.
Pu R, Gong P, Michishita R, Sasagawa T. 2006. Assessment of multi-resolution and multi-sensor data for urban surface temperature retrieval. *Remote Sensing of Environment* **104**: 211–225.
Rajasekar U, Weng Q. 2008. Urban heat island monitoring and analysis using a non-parametric model: a case study of Indianapolis. *ISPRS Journal of Photogrammetry and Remote Sensing* **64**: 86–96.
Retalis A, Paronis D, Lagouvardos K, Kotroni V. 2010. The heat wave of June 2007 in Athens, Greece – part 1: study of satellite derived land surface temperature. *Atmospheric Research* **98**: 458–467.
Rigo G, Parlow E, Oesch D. 2006. Validation of satellite observed thermal emission with in-situ measurements over an urban surface. *Remote Sensing of Environment* **104**: 201–210.
Rizwan A, Dennis L, Liu C. 2008. A review on the generation, determination and mitigation of urban heat island. *Journal of Environmental Sciences* **20**: 120–128.
Roberts JJ, Best BD, Dunn DC, Treml EA, Halpin PN. 2010. Marine geospatial ecology tools: an integrated framework for ecological geoprocessing with ArcGIS, Python, R, MATLAB, and C++. *Environmental Modelling and Software* **25**: 1197–1207.
Sandau R, Brieß K, Derrico M. 2010. Small satellites for global coverage: potential and limits. *ISPRS Journal of Photogrammetry and Remote Sensing* **65**: 492–504.
Schmetz J, Pili P, Tjemkes S, Just D, Kerkmann J, Rota S, Ratier A. 2002. Supplement to an introduction to meteosat second generation (MSG). *Bulletin of the American Meteorological Society* **83**: 992–992.
Senay GB, Budde M, Verdin JP, Melesse AM. 2007. A coupled remote sensing and simplified surface energy balance approach to estimate actual evapotranspiration from irrigated fields. *Sensors* **7**: 979–1000.
Sobrino J. 2004. Land surface temperature retrieval from MSG1-SEVIRI data. *Remote Sensing of Environment* **92**: 247–254.
Sobrino J, Jimenez-Munoz J, Zarco-Tejada P, Sepulcre-Canto G, Miguel E. 2006. Land surface temperature derived from airborne hyperspectral scanner thermal infrared data. *Remote Sensing of Environment* **102**: 99–115.
Sòria G, Sobrino J. 2007. ENVISAT/AATSR derived land surface temperature over a heterogeneous region. *Remote Sensing of Environment* **111**: 409–422.
Stathopoulou M, Cartalis C. 2007. Daytime urban heat islands from Landsat ETM+ and Corine land cover data: an application to major cities in Greece. *Solar Energy* **81**: 358–368.
Stathopoulou M, Cartalis C. 2009. Downscaling AVHRR land surface temperatures for improved surface urban heat island intensity estimation. *Remote Sensing of Environment* **113**: 2592–2605.
Stathopoulou M, Cartalis C, Chrysoulakis N. 2006. Using midday surface temperature to estimate cooling degree-days from NOAA-AVHRR thermal infrared data: an application for Athens, Greece. *Solar Energy* **80**: 414–422.
Stewart I. 2010. A systematic review and scientific critique of methodology in modern urban heat island literature. *International Journal of Climatology* **31**: 200–217.
Streutker D. 2003. Satellite-measured growth of the urban heat island of Houston, Texas. *Remote Sensing of Environment* **85**: 282–289.
Sun D. 2003. Estimation of land surface temperature from a Geostationary Operational Environmental Satellite (GOES-8). *Journal of Geophysical Research* **108**: 1–15.
Sun D, Pinker R, Basara J. 2004. Land surface temperature estimation from the next generation of geostationary operational environmental satellites: GOES M–Q. *Journal of Applied Meteorology* **43**: 363–372.
Sun D, Pinker RT, Kafatos M. 2006. Diurnal temperature range over the United States: a satellite view. *Geophysical Research Letters* **33**: 1–4.
Tomlinson C, Chapman L, Thornes J, Baker C. Derivation of Birmingham's summer surface urban heat island from MODIS satellite images. *International Journal of Climatology* (in press).
Trigo IF, Monteiro IT, Olesen F, Kabsch E. 2008. An assessment of remotely sensed land surface temperature. *Journal of Geophysical Research* **113**: 1–12.
Ulivieri C, Cannizzaro G. 1985. Land surface temperature retrievals from satellite measurements. *Acta Astronautica* **12**: 977–985.
Umamaheshwaran R, Bijker W, Stein A. 2007. Image mining for modeling of forest fires from meteosat images. *IEEE Transactions on Geoscience and Remote Sensing* **45**: 246–253.
Vancutsem C, Ceccato P, Dinku T. 2010. Evaluation of MODIS land surface temperature data to estimate air temperature in different ecosystems over Africa. *Remote Sensing of Environment* **114**: 449–465.
Vázquez DP, Reyes FJO, Arboledas LA. 1997. A comparative study of algorithms for estimating land surface temperature from AVHRR data. *Remote Sensing of Environment* **62**: 215–222.
Voogt J, Oke T. 2003. Thermal remote sensing of urban climates. *Remote Sensing of Environment* **86**: 370–384.
Wan Z. 2002. Validation of the land-surface temperature products retrieved from terra moderate resolution imaging Spectroradiometer data. *Remote Sensing of Environment* **83**: 163–180.
Wan Z. 2008. New refinements and validation of the MODIS land-surface temperature/emissivity products. *Remote Sensing of Environment* **112**: 59–74.
Wan Z, Dozier J. 1996. A generalized split-window algorithm for retrieving land-surface temperature from space. *IEEE Transactions on Geoscience and Remote Sensing* **34**: 892–905.

Wan Z, Zhang Y, Zhang Q, Li Z. 2004. Quality assessment and validation of the MODIS global land surface temperature. *International Journal of Remote Sensing* **25**: 261–274.

Wang K, Liang S. 2009. Evaluation of ASTER and MODIS land surface temperature and emissivity products using long-term surface long wave radiation observations at SURFRAD sites. *Remote Sensing of Environment* **113**: 1556–1565.

Weller J, Thornes JE. 2001. An investigation of winter nocturnal air and road surface temperature variation in the West Midlands, UK under different synoptic conditions. *Meteorological Applications* **8**: 461–474.

Weng Q. 2003. Fractal analysis of satellite-detected urban heat island effect. *Photogrammetric Engineering and Remote Sensing* **69**: 555–566.

Weng Q. 2009. Thermal infrared remote sensing for urban climate and environmental studies: methods, applications, and trends. *ISPRS Journal of Photogrammetry and Remote Sensing* **64**: 335–344.

Weng Q, Lu D, Schubring J. 2004. Estimation of land surface temperature-vegetation abundance relationship for urban heat island studies. *Remote Sensing of Environment* **89**: 467–483.

Williams CN, Basist A, Peterson TC, Grody N. 2000. Calibration and verification of land surface temperature anomalies derived from the SSM/I. *Bulletin of the American Meteorological Society* **81**: 2141–2156.

Xian G, Crane M. 2006. An analysis of urban thermal characteristics and associated land cover in Tampa Bay and Las Vegas using Landsat satellite data. *Remote Sensing of Environment* **104**: 147–156.

Yamaguchi Y, Kahle AB, Tsu H, Kawakami T, Pniel M. 1998. Overview of advanced spaceborne thermal emission and reflection radiometer (ASTER). *IEEE Transactions on Geoscience and Remote Sensing* **36**: 1062–1071.

Yan H, Zhang J, Hou Y, He Y. 2009. Estimation of air temperature from MODIS data in east China. *International Journal of Remote Sensing* **30**: 6261–6275.

Yu Y, Privette JL, Pinheiro AC. 2008. Evaluation of split-window land surface temperature algorithms for generating climate data records. *IEEE Transactions on Geoscience and Remote Sensing* **46**: 179–192.

Yunyue Y, Tarpley D, Privette JL, Goldberg MD, Rama Varma Raja MK, Vinnikov KY, Hui X. 2009. Developing algorithm for operational GOES-R land surface temperature product. *IEEE Transactions on Geoscience and Remote Sensing* **47**: 936–951.

